

# Layer Thickness-Dependent Hardness and Strain Rate Sensitivity of Cu–Al/Al Nanostructured Multilayers

Ya-Qiang Wang<sup>1</sup> · Zhao-Qi Hou<sup>1</sup> · Jin-Yu Zhang<sup>1</sup> · Xiao-Qing Liang<sup>1</sup> · Gang Liu<sup>1</sup> · Guo-Jun Zhang<sup>2</sup> · Jun Sun<sup>1</sup>

Received: 18 August 2015/Revised: 6 November 2015/Published online: 20 January 2016  
© The Chinese Society for Metals and Springer-Verlag Berlin Heidelberg 2016

**Abstract** Cu–Al/Al nanostructured metallic multilayers with Al layer thickness  $h_{\text{Al}}$  varying from 5 to 100 nm were prepared, and their mechanical properties and deformation behaviors were studied by nanoindentation testing. The results showed that the hardness increased drastically with decreasing  $h_{\text{Al}}$  down to about 20 nm, whereafter the hardness reached a plateau that approaches the hardness of the alloyed Cu–Al monolithic thin films. The strain rate sensitivity (SRS,  $m$ ), however, decreased monotonically with reducing  $h_{\text{Al}}$ . The layer thickness-dependent strengthening mechanisms were discussed, and it was revealed that the alloyed Cu–Al nanolayers dominated at  $h_{\text{Al}} \leq 20$  nm, while the crystalline Al nanolayers dominated at  $h_{\text{Al}} > 20$  nm. The plastic deformation was mainly related to the ductile Al nanolayers, which was responsible for the monotonic evolution of SRS with  $h_{\text{Al}}$ . In addition, the  $h_{\text{Al}}$ -dependent hardness and SRS were quantitatively modeled in light of the strengthening mechanisms at different length scales.

**KEY WORDS:** Nanostructured films; Cu–Al/Al multilayers; Hardness; Strain rate sensitivity; Layer thickness dependence

## 1 Introduction

Nanostructure metallic multilayers (NMMs) are made up of alternating nanometer-scale layers of two or more different materials, where the individual layer thickness can be varied from a few atomic layers to hundreds of nanometers. These NMMs offer outstanding mechanical properties, such as superior strength/hardness, high

toughness and great radiation tolerance suitable for applications, which are far different from their bulk counterparts [1–7]. For example, the Cu/Al [8] and Ag/Al [8] NMMs composed of two soft phases exhibit greatly enhanced strength compared with their corresponding constituents (i.e., Cu, Al and Ag). These outstanding properties are related to the abundant homogeneous boundaries (e.g., grain boundaries, GBs and twin boundaries, TBs)/heterophase interfaces and nanoscale effects associated with structural peculiarities of nanostructured materials, e.g., small intrinsic size (including grain size  $d$ , twin thickness  $\lambda$ , layer thickness  $h$ ) less than 100 nm. The strength/hardness of NMMs in general exhibits the fashion of smaller is stronger, i.e., their strength/hardness increases with decreasing layer thickness  $h$  to several nanometers  $\sim 2$ –5 nm [2, 4, 9, 10]. These size-dependent strengthening mechanisms of NMMs have been widely explained by several phenomenological strengthening models at different length scales [11]: (i) the H–P-like strengthening relationship based on piling-up of dislocations against the

Available online at <http://link.springer.com/journal/40195>

✉ Gang Liu  
lgsammer@mail.xjtu.edu.cn

✉ Jun Sun  
junsun@mail.xjtu.edu.cn

<sup>1</sup> State Key Laboratory for Mechanical Behavior of Materials, Xi'an Jiaotong University, Xi'an 710049, China

<sup>2</sup> School of Materials Science and Engineering, Xi'an University of Technology, Xi'an 710048, China

interface, which is applicable at the sub-micrometer to micron scales, (ii) the confined layer slip (CLS) mechanism involving single dislocation loop glide confined to isolated layers, which works at few to a few tens of nanometers scales, and (iii) the interface barrier strength (IBS) mechanism in consideration of single dislocation cutting cross the interface, which is operative at a few nanometers scales. On the other hand, the strain rate sensitivity (SRS,  $m$ ) of NMMs has been investigated recently. It is unveiled that the index of SRS of Cu/ $X$  ( $X = \text{Cr, Zr, Cu-Zr}$ ) NMMs [2, 12, 13] monotonically increases with decreasing layer thickness  $h$ , similar to that of Cu. The elevated SRS  $m$  of the Cu/ $X$  NMMs can be attributed to the transition from dislocation slip in the isolated layer at large layer thickness  $h$  to dislocation cutting across the interface at small layer thickness  $h$  [3].

Tuning the internal size/feature at the nanoscale to control the mechanical properties of Cu-based metals has attracted extensive attention [14, 15] and becomes a universal strategy among material scientists and engineers, since plastic characteristics (i.e., strength, strain rate sensitivity and activation volume) of nanomaterials are highly sensitive to their microstructures. Recently, our experimental findings [14] have clearly uncovered that lowering the stacking fault energy (SFE) in micron-thick Cu thin films via Al microalloying can significantly introduce abundance of nanotwins into these Cu thin films (with Al addition of only 4 at%) and result in a remarkable strengthening response. It is thus natural to ask whether the superior strength of alloyed Cu–Al thin films can be retained or even further enhanced when laminating soft and light metals, such as Al, with the Cu–Al layers to lower the weight of Cu-based materials. Specifically, the nanolayered architecture not only provides an effective way to tailor the geometric and microstructural length of the materials, but also makes the multilayers become ideal model materials to investigate the length scale-dependent plasticity of thin films at nanoscale, in particular under strong size and interface constraining conditions. Also, it is quite important to know whether or not the Al nanolayers can influence the microstructure and resultant mechanical properties of Cu–Al nanolayers during the Cu–Al/Al NMMs preparation.

In this work, the Cu–Al/Al NMMs with constant Cu–Al layer thickness of  $\sim 100$  nm but different Al layer thicknesses spanning from 5 to 100 nm were selected as the studied materials. Employing the traditional nanoindentation test, we measured the hardness and SRS of the Cu–Al/Al NMMs and uncovered that their hardness increases generally with thinning the Al layers, whereas their SRS decreases with reducing Al layer thickness. The high strength and low SRS of Cu–Al/Al NMMs at small length provide new insights into tuning the plasticity of NMMs via the microalloying method.

## 2 Experimental

Cu–Al/Al NMMs were deposited on HF-etched (100) Si wafers substrates by direct current magnetron sputtering at room temperature. Targets of pure Cu (99.995%) and Al (99.995%) were used to prepare alternating nanolayers of alloyed Cu-4 at% Al and pure Al. The chamber was evacuated to a base pressure of  $3.6 \times 10^{-7}$  Torr ( $4.8 \times 10^{-5}$  Pa), and  $8.3 \times 10^{-3}$  Torr (1.1 Pa) of Ar was maintained during the deposition process. The substrate was neither heated nor cooled during the deposition process. The Cu–Al/Al NMMs have a constant alloyed Cu–Al layer thickness of  $\sim 100$  nm but different crystalline Al layer thicknesses ranging from 5 to 100 nm. The total thickness of all the NMMs is  $\sim 2.0$   $\mu\text{m}$ , containing 10 modulations for the 100 nm Cu–Al/100 nm Al samples (hereafter referred to as the Cu–Al/Al-100) and 20 modulations for the Cu–Al/Al-5 ones. For comparison, the 2.0- $\mu\text{m}$ -thick Cu-4 at% Al and pure Al thin films were also prepared on Si substrates. To examine the phase structure and crystallographic texture, X-ray diffraction (XRD) experiments were performed using a Bruker D8 Discover powder X-ray diffractometer with CuK $\alpha$  radiation at room temperature. Transmission electron microscopy (TEM) and energy-dispersive X-ray (EDX) analyses were conducted using a JEOL JEM-2100F microscope to identify the microstructure and the elemental composition of the specimens.

Nanoindentation measurements were performed on all the film materials deposited on Si substrate by using a TI950 TriboIndenter (Hysitron, Minneapolis, MN) with a standard Berkovich tip at room temperature. The nanoindentation data were collected within a maximum indenting depth of 10%–15% of the whole thickness for each specimen to eliminate the substrate effects [16]. The hardness test was carried out on the load-controlled mode for all the Cu–Al/Al NMMs (4000  $\mu\text{N}$ ). A minimum of 9 indents was performed on each specimen to obtain average and standard deviations for hardness. To improve the reliability and accuracy of the present measurements, great efforts were devoted to the correction of thermal drift in the nanoindentation test. In the present study, the allowable drift rate was set at  $0.01 \text{ nm s}^{-1}$ , which is tenfold smaller than the typical value ( $0.1 \text{ nm s}^{-1}$ ) generally used in typical nanoindentation tests. To evaluate the SRS  $m$  of the Cu–Al/Al NMMs, the hardness of specimens was measured at different strain rates  $\dot{\epsilon}$  defined by [17]

$$\dot{\epsilon} = \frac{\dot{P}}{2P}, \quad (1)$$

where  $P$  is the load and  $\dot{P} = dP/dt$  is the loading rate. In this study, the nanoindentation tests were carried out at four different strain rates of 0.01, 0.05, 0.1 and  $0.25 \text{ s}^{-1}$  on the Cu–Al/Al NMMs. The SRS  $m$  is experimentally

defined as the slope of the double logarithmic plot of hardness  $H$  and strain rates  $\dot{\epsilon}$  under isothermal conditions, which can be expressed as:

$$m = \frac{\partial \log(H)}{\partial \log(\dot{\epsilon})}. \quad (2)$$

### 3 Results and Discussion

#### 3.1 Microstructure of the Cu–Al/Al NMMs

High-angle XRD spectra for all the as-deposited Cu–Al/Al NMMs are displayed in Fig. 1 for comparison. The Cu–Al/Al NMMs show Cu-(111), Al-(111), Cu-(200) and Al-(200) texture, but the diffraction peaks of Al layers are relatively weaker as the thickness of Al layer is thinner.

Figure 2 shows the representative cross-sectional TEM and high-resolution TEM (HRTEM) images of the as-deposited Cu–Al/Al-50 NMMs. The modulated layered structure with clear interfaces between alloyed Cu–Al and nanocrystalline Al nanolayers can be observed. The grain size of Cu–Al nanolayers almost equals the layer thickness of  $\sim 100$  nm; while that of Al nanolayers is smaller than the thickness at large length  $h > 20$  nm, below which the grain size scales with the layer thickness. The selected area electron diffraction (SAED) pattern in Fig. 2a definitely demonstrates Al-(111) and Al-(200) textures as well as Cu-(111) and Cu-(200) textures, which are consistent with the XRD results. Abundance of nanotwins and stacking faults exists in the Cu–Al nanolayers. The fraction of twinned grains is up to  $\sim 45\%$ , close to our previous reports in the 2- $\mu\text{m}$ -thick Cu-4 at% Al thin films [14]. This implies that the Al nanolayers have negligible effect on the formation of nanotwins and/or stacking faults in the Cu–Al layers. Figure 3 shows the typical EDX mapping analysis of the Cu–Al/Al-50 NMMs. The EDX result of the rectangle

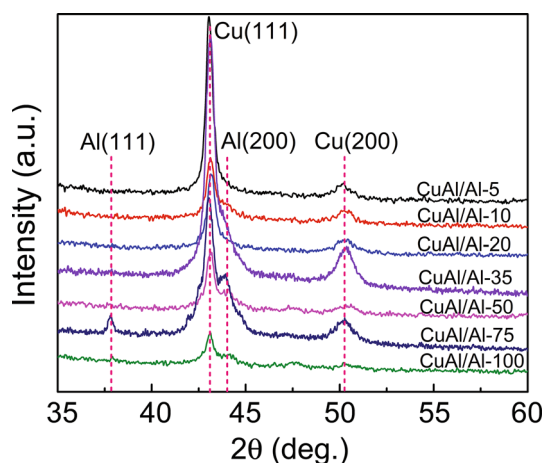


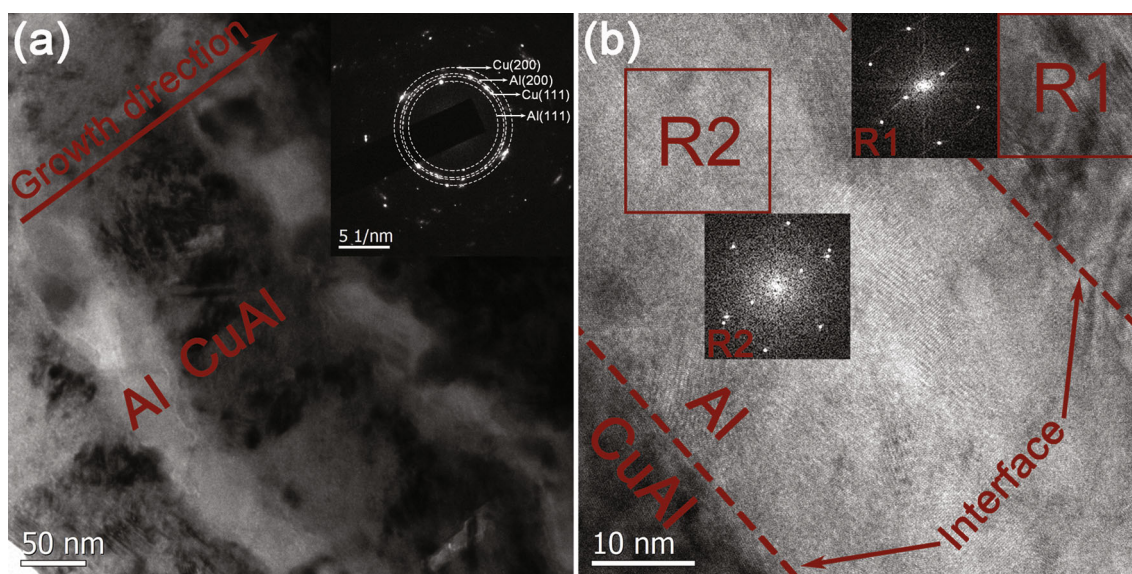
**Fig. 1** XRD patterns for the Cu–Al/Al NMMs with different thicknesses of Al layer  $h_{\text{Al}}$

region in Fig. 3a still reveals the chemical modulation structure, as displayed in Fig. 3b, c.

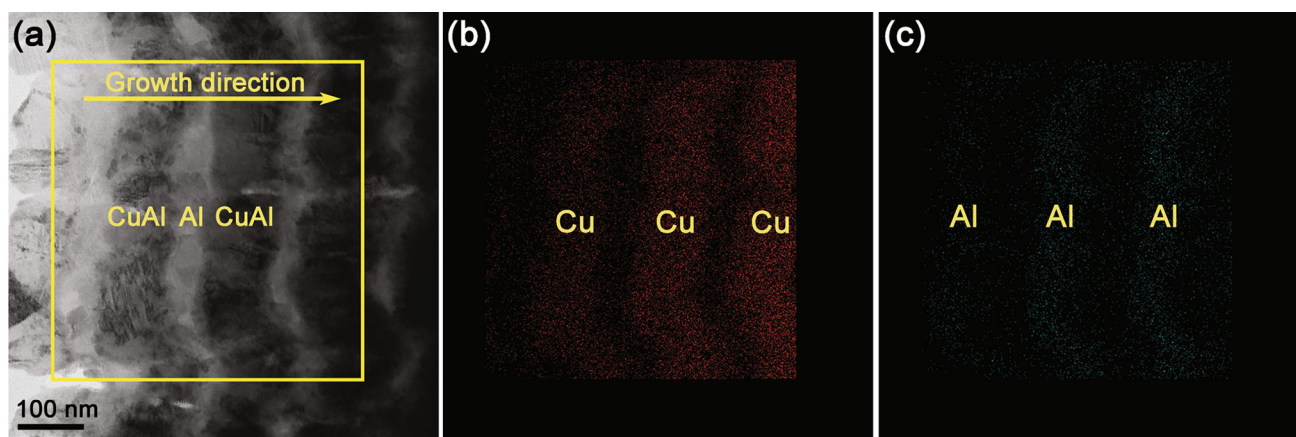
#### 3.2 Hardness of the Cu–Al/Al NMMs

Figure 4a, b presents the representative nanoindentation load–depth curves of Cu–Al/Al NMMs with  $h_{\text{Al}} = 20$  nm at different strain rates and all the Cu–Al/Al NMMs at strain rate of  $0.1 \text{ s}^{-1}$ , respectively. All the curves manifest the smooth mechanical response without notable discrete burst of rapid displacement under the load-controlled mode. Taking the Cu–Al/Al-20 NMMs for example, the indentation depth decreases with increasing loading rate (Fig. 4a), implying a positive SRS in the present Cu–Al/Al NMMs. In addition, the indentation depth monotonically decreases with decreasing Al layer thickness of Cu–Al/Al NMMs (Fig. 4b), indicating an increased hardness with reducing Al layer thickness.

The upper part of Fig. 5 shows the indentation hardness of Cu–Al/Al NMMs as a function of Al layer thickness  $h_{\text{Al}}$ . It can be seen that the hardness of Cu–Al/Al NMMs drastically increases from  $\sim 3.2$  to  $\sim 4.8$  GPa as  $h_{\text{Al}}$  decreasing from 100 to  $\sim 20$  nm (in regime II) and then reaches a hardness plateau of  $\sim 4.8$  GPa with further decreasing  $h_{\text{Al}}$  to 5 nm (in regime I). This hardness–size relation of Cu–Al/Al NMMs is quite similar to the case of reported Cu/Al NMMs, as displayed in the bottom part of Fig. 5, which shows a quite low hardness plateau of  $\sim 1.8$  GPa at small  $h_{\text{Al}} \leq 70$  nm [8], as well as other reported Cu-based NMMs such as Cu/Zr [18], Cu/Ni [19] and Cu/Fe [20]. It seems that, compared with the Cu/Al NMMs [8], the present Cu–Al/Al samples exhibit greater enhancement in hardness via microalloying the Cu nanolayers with Al at the identical internal size  $h$ . To more clearly clarify this layer thickness-dependent plasticity, we divided this hardness–layer thickness map of Fig. 5 into two regimes, i.e., regime I at  $h_{\text{Al}} \leq 20$  nm and regime II at  $h_{\text{Al}} > 20$  nm. In regime I, the saturation hardness ( $\sim 4.8$  GPa) of Cu–Al/Al NMMs is nearly the same as that of alloyed monolithic Cu-4 at% Al thin films but is far greater than that of pure nanocrystalline Al thin films  $\sim 1.8$  GPa, implying alloyed Cu–Al nanolayers possibly dominate the plastic deformation of NMMs due to their high volume fraction. Even though the Al layers have a larger value of hardness compared to the 100 nm Cu–Al layers due to the smaller layer thickness, they play little role in the mechanical performance for their less volume fraction. Therefore, the hardness of NMMs is close to the monolithic Cu-4 at% Al thin films. By contrast, in regime II, nanocrystalline Al layers as the soft phase dominate the plastic deformation of NMMs, and their effect becomes more and more significant with increasing  $h_{\text{Al}}$  (i.e., the volume fraction of Al layers). In the following, we



**Fig. 2** Representative TEM **a**, HRTEM **b** images of as-deposited Cu–Al/Al NMMs with  $h_{\text{Al}}$  of 50 nm. The SAED inset in **a** exhibits the strong Cu (111), Cu (200) and Al (111), Al (200) texture. Fast Fourier transform (FFT) from two interest regions RI (in the Cu–Al layer) and RII (in the Al layer) in **b** indicate the fcc crystalline structure



**Fig. 3** **a** Typically EDX mapping analysis of the Cu–Al/Al NMMs with  $h_{\text{Al}}$  of 50 nm, **b**, **c** show the uniform distribution of constituent elements

quantitatively elucidated the underlying mechanisms for the layer thickness-independent hardness in regime I and layer thickness-dependent hardness in regime II, respectively, by considering the hardness discrepancy between the Cu–Al and Al nanolayers.

To begin with, we simply treat the Cu–Al/Al NMMs as composites consisting of two different crystalline phases, i.e., the soft Al phase and hard Cu–Al alloyed phase, and the hardness of the Cu–Al/Al NMMs can be estimated by assuming the effective medium theory is still operative in the nanoscale:

$$H = H_{\text{CuAl}} \frac{h_{\text{CuAl}}}{h_{\text{CuAl}} + h_{\text{Al}}} + H_{\text{Al}} \frac{h_{\text{Al}}}{h_{\text{CuAl}} + h_{\text{Al}}}. \quad (3)$$

where  $H_{\text{CuAl}}$  ( $h_{\text{CuAl}}$ ) and  $H_{\text{Al}}$  ( $h_{\text{Al}}$ ) are the hardness (layer thickness) of alloyed Cu–Al and nanocrystalline Al

nanolayers, respectively. Since the alloyed Cu–Al nanolayers have a constant thickness of  $\sim 100$  nm in the Cu–Al/Al NMMs, we can approximately take  $H_{\text{CuAl}}$  as  $\sim 4.8$  GPa. Following the well-known relation of  $H_{\text{Al}} = 2.7\sigma_{\text{Al}}$ , next we will evaluate the strength of Al nanolayers  $\sigma_{\text{Al}}$  as a function of its thickness  $h_{\text{Al}}$ .

In Al nanolayers, with the thickness  $h_{\text{Al}}$  reducing to the nanoscale, dislocations no longer generate from sources in the interior of the grains, while instead emit from the GBs. Thus, the hardness of Al nanolayers can be theoretically calculated in terms of the GBs dislocations activities at such length scale by considering the transition from partials to full dislocations emission. It is well established that the required stress to emit Shockley partials ( $\sigma_{\text{P}}$ ) and full dislocations ( $\sigma_{\text{F}}$ ) from GBs can be, respectively, expressed as [19, 21–23]

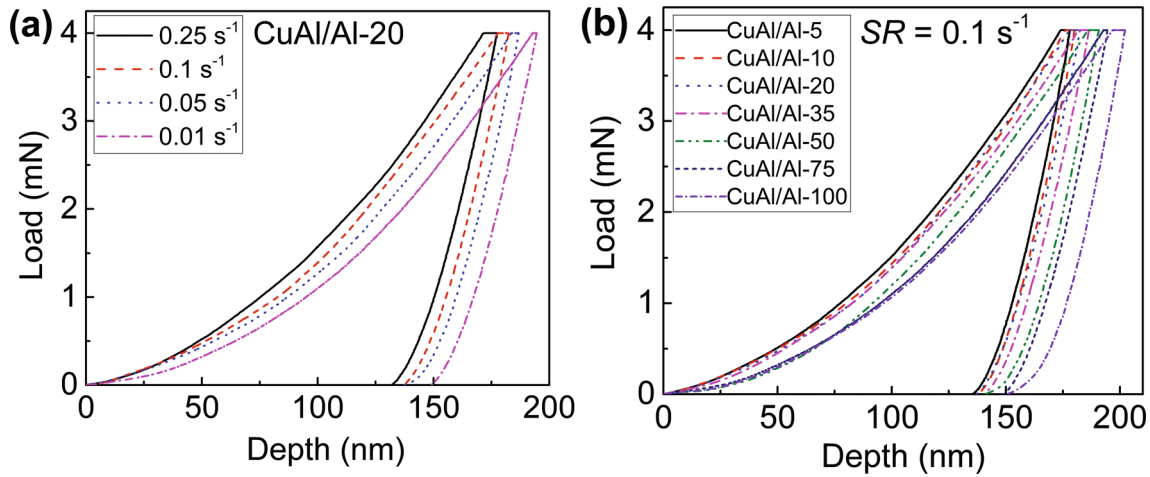


**Fig. 4** Representative load–depth curves of Cu–Al/Al NMMs with  $h_{Al}$  of 20 nm at different strain rates **a**, all the Cu–Al/Al NMMs at strain rate of  $0.1 \text{ s}^{-1}$  **b**

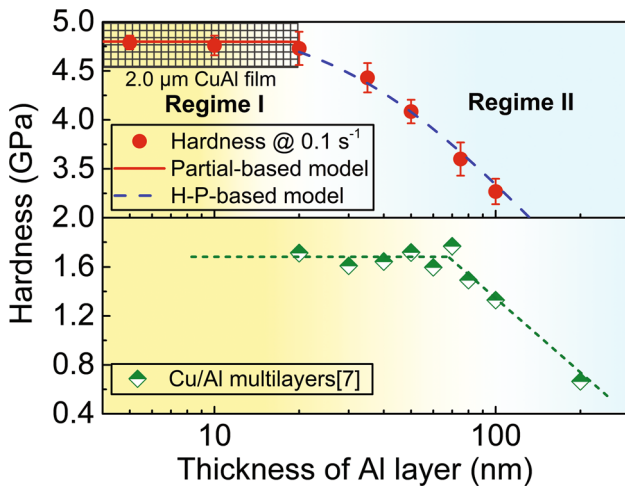


**Fig. 5** Dependence of nanoindentation hardness on  $h_{Al}$  for Cu–Al/Al NMMs (*upper part*) and Cu/Al multilayers (*bottom part*) [8]

$$\sigma_P = \frac{1}{m \cdot s} \left( \frac{\gamma_{Al} - \gamma_{CuAl}}{b_P} + \frac{R\mu_{Al} \sin \varphi}{8\pi} \right), \quad (4)$$

where the first term is a consequence of differences in SFE of the constituent layers and the second term is the modulus mismatch-induced repulsive image force, and

$$\sigma_F = \frac{1}{s} \frac{2\alpha\mu_{Al}b_F}{h_{Al}}, \quad (5)$$

where  $s \sim 0.27\text{--}0.41$  is the Schmid factor of the corresponding slip system [21],  $R = (\mu_{Al} - \mu_{CuAl}) / (\mu_{Al} + \mu_{CuAl})$ ,  $\mu_{Al} \sim 26 \text{ GPa}$  and  $\mu_{CuAl} \sim 48 \text{ GPa}$  is the shear modulus of Al and alloyed Cu–Al, respectively,  $\varphi \sim 70.5^\circ$ ,  $\gamma$  is the stacking fault energy (SFE,  $\sim 140 \text{ mJ/m}^2$  for Al and  $\sim 30 \text{ mJ/m}^2$  for Cu-4 at% Al),  $m \sim 2\text{--}4$  is a stress concentration factor [23], the parameter  $\alpha$  reflects the

character of the dislocation ( $\alpha = 0.5$  and  $1.5$  for edge and screw dislocations, respectively) [22, 23],  $b_F (= 0.286 \text{ nm})$  and  $b_P (= 0.165 \text{ nm})$  are the magnitude of the Burgers vector of the full and partial dislocations, respectively. Therefore, the critical value  $h_c$  calculated by equating Eqs. (4) and (5) determines the transition from partials emission to full dislocations emission, which is given by

$$h_c = \frac{2\alpha m \mu_{Al} b_F}{\frac{\gamma_{Al} - \gamma_{CuAl}}{b_P} + \frac{R\mu_{Al} \sin \varphi}{8\pi}}. \quad (6)$$

Taking  $\alpha = 1.0$  and  $m = 2.0$ , the estimated critical layer thickness  $h_c$  is approximately 30 nm for aluminum. Therefore, when the Al layer thickness  $h_{Al} < h_c$ , the above-mentioned partial dislocation model can be used to describe the strength of Al layers in Cu–Al/Al NMMs; otherwise, the full dislocation mechanism works. Actually, the calculated hardness of Al nanolayers from Eq. (4) at such length is about  $H_{Al} = 2.7\sigma_{Al} \approx 4.78 \text{ GPa}$ , almost equaling that of Cu–Al alloyed nanolayers. It is suggested that both the Cu–Al and Al nanolayers co-deform at small length scale in regime I. Substituting Eq. (4) into Eq. (3), the calculations on  $h_{Al}$ -independent hardness of Cu–Al/Al NMMs are in good agreement with the experimental results (see the red solid line in Fig. 5).

By contrast, in regime II ( $h_{Al} > 20 \text{ nm}$ ), the thickness of crystalline Al layer is larger in this regime and dislocations will pile up against the interface; therefore, the H–P model can be used to evaluate the strength of Al nanolayers  $\sigma_{Al}$ , given by [18, 24]

$$\sigma_{Al} = \sigma_0 + k \cdot h_{Al}^{-1/2}. \quad (7)$$

where  $\sigma_0$  is the lattice friction stress ( $\sim 0.01 \text{ GPa}$ ) [25] and  $k$  is the H–P slope which is considered to be a measure of the resistance of the GB against transfer ( $\sim 6.85 \text{ GPa nm}^{1/2}$ ).

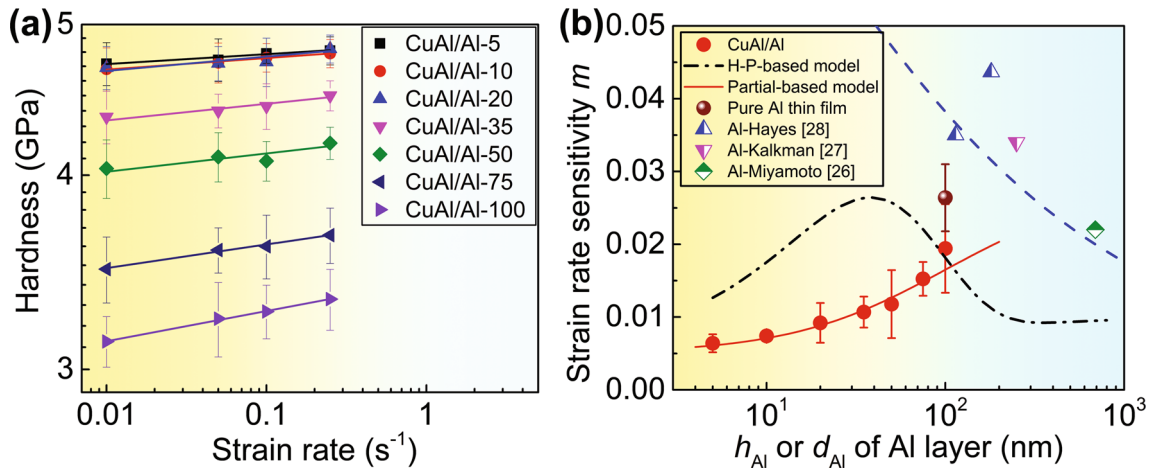


**Fig. 6** **a** Representative log*H* versus log  $\dot{\epsilon}$  plots of Cu–Al/Al NMMs with different *h*<sub>Al</sub>, **b** experimental results of the strain rate sensitivity *m* as a function of *h*<sub>Al</sub> for the Cu–Al/Al NMMs

Similarly, submitting Eq. (7) into Eq. (3), the calculated hardness of CuAl/Al NMMs can be in good agreement with the experimental results (see the blue dash line in Fig. 5).

### 3.3 Strain rate sensitivity of the Cu–Al/Al NMMs

Figure 6a summarizes the strain rate-dependent hardness of Cu–Al/Al NMMs at different thicknesses of *h*<sub>Al</sub>. It appears that faster strain rates result in higher hardness, indicative of the positive SRS. In these log–log plots between hardness and strain rates, all the strain rate dependences are clearly linear, which guarantees the evaluation of *m*. We can see that the slope of the fitted linear is higher at larger *h*<sub>Al</sub> and almost remains a constant at smaller *h*<sub>Al</sub>. Figure 6b clearly describes the relationship between *m* of CuAl/Al NMMs and *h*<sub>Al</sub>. It seems that the measured *m* decreases gradually from 0.02 to 0.006 with *h*<sub>Al</sub> reducing from 100 to 5 nm, lower than that (*m*<sub>Al</sub> ~ 0.025) of pure nanocrystalline Al thin film with grain size of ~ 100 nm. This trend seems to indicate that the Al nanolayers dominate the SRS in the studied length scale, which is just contrary to the tendency of layer thickness-dependent SRS of pure Al [26–28] that monotonically increases with decreasing internal characteristic size (see the blue dash line in Fig. 6b). In our previous work [3, 18, 29], we have uncovered that the SRS *m* of Cu/*X* (*X* = Cr, Zr) with equal layer thickness monotonically increases with decreasing layer thickness of Cu, implying the size or interface density controls the SRS. By contrast, the SRS *m* of Cu/*X* with unequal layer thickness (but constant modulation period of ~ 50 nm) monotonically increases with increasing Cu layer thickness (or Cu volume fraction), implying the deformable phase volume fraction controls the SRS. Unlike these two cases, in the present Cu–Al/Al NMMs the SRS *m* increases simultaneously with increasing Al volume fraction and decreasing

interface density. This finding suggests that it is the softer phase that dominates the SRS of Cu–Al/Al NMMs.

It is well known that SRS *m* is a parameter to characterize the strain rate dependence of hardness. In the Al nanolayers, above discussion has revealed that the flow stress is controlled by the partials emitted from the GBs. Based on the partials’ emission-controlled strengthening mechanism, a mechanistic model proposed by Gu *et al.* [30] was initially used to quantitatively describe the layer thickness-dependent SRS in nanocrystalline metals and subsequently applied to crystalline NMMs [3]. According to this model, the critical dislocation half-circular loop size for activation (*r*<sub>c</sub>) in the Al nanolayers can be given as follows by referring to [30]

$$r_c = \kappa \left( \frac{\tau_{Al}}{\mu} \right)^{-1} b_p \left( \ln \frac{\sqrt{3} r_c}{b_p} + 1 \right), \quad (8)$$

where  $\kappa$  is the dislocation nucleation factor that has a value of about 0.04 in the case of inhomogeneous nucleation [30], and the shear flow stress  $\tau_{Al}$  is given by Eq. (4) at small size scale (partial-based model) and Eq. (7) at large size scale (H–P-based model), respectively. The activation volume is obtained by [30]

$$V^* = \frac{1}{2} \pi (r_c)^2 b_p. \quad (9)$$

and the strain rate sensitivity *m*<sub>Al</sub> is related to *V*<sup>\*</sup> by the expression [31, 32]

$$m_{Al} = \frac{k_B T}{\tau_{Al} \cdot V^*}. \quad (10)$$

where *k*<sub>B</sub> is the Boltzmann constant and *T* is the absolute temperature.

Similar to the case of layer thickness-dependent hardness, the rule of mixtures can be adopted to quantitatively

understand the influences of constituent nanolayers on the SRS via the equation:

$$m = m_{\text{CuAl}} \frac{h_{\text{CuAl}}}{h_{\text{CuAl}} + h_{\text{Al}}} + m_{\text{Al}} \frac{h_{\text{Al}}}{h_{\text{CuAl}} + h_{\text{Al}}}. \quad (11)$$

where  $m_{\text{CuAl}}$  and  $m_{\text{Al}}$  are the SRS of Al and Cu–Al thin films, respectively. As the thickness of alloyed Cu–Al layer is constant ( $\sim 100$  nm), we then simply take the SRS  $m_{\text{CuAl}}$  as a constant. Substituting Eq. (10) into Eq. (11), one can see that the measured SRS  $m$  of Cu–Al/Al NMMs can be captured at the small size scale ( $h_{\text{Al}} \leq 50$  nm) via the partial-based model, as depicted in Fig. 6b by the red solid line, using  $m_{\text{CuAl}} \sim 0.005$  that almost equals that of the 2.0- $\mu\text{m}$ -thick Cu–4 at% Al within the scatter. At the large scale ( $h_{\text{Al}} > h_{\text{c}}$ ), full dislocations are emitted from the GBs. In such case, the shear flow stress  $\tau_{\text{Al}}$  estimated from the H–P model should be used to calculate the SRS  $m$  of Cu–Al/Al NMMs. By combining Eqs. (7)–(10) and replacing  $b_{\text{P}}$  with  $b_{\text{F}}$ , it was found that the H–P-based model overestimated the SRS  $m$  of Cu–Al/Al NMMs at small size scale and captured the experimental results at the large size scale  $h_{\text{Al}} > 50$  nm (see the black dash dot line in Fig. 6b), implying the limitation of H–P model in nanoscale.

## 4 Conclusion

This work experimentally studied the hardness and the SRS of a series of Cu–Al/Al multilayers with Al layer thickness  $h_{\text{Al}}$  ranging from 5 to 100 nm. With reducing  $h_{\text{Al}}$ , the hardness first increased dramatically and then reached a plateau of about 4.8 GPa at  $h_{\text{Al}}$  below  $\sim 20$  nm. This is because alloyed Cu–Al nanolayers and crystalline Al nanolayers co-deform contributing to the plastic deformation of Cu–Al/Al NMMs at smaller  $h_{\text{Al}}$ , while Al nanolayers as the soft phase dominate the plastic deformation of Cu–Al/Al NMMs at larger  $h_{\text{Al}}$ . A decreased SRS  $m$  of Cu–Al/Al multilayers with reducing  $h_{\text{Al}}$  revealed the dominant role of the softer Al phase played in the layer thickness-dependent SRS. Both the layer thickness-dependent hardness and SRS were quantitatively explained by the partial-based model and H–P-based model, which operate at different length scales.

**Acknowledgments** This work was supported by the National Natural Science Foundation of China (Grant Nos. 51321003, 51322104 and 51201123), the National Basic Research Program of China (Grant No. 2010CB631003) and the 111 Project of China (Grant No. B06025). G. Liu thanks the support from the Fundamental Research Funds for the Central Universities and the Tengfei Scholar project. J.Y. Zhang thanks the Natural Science Basic Research Plan in Shaanxi Province of China (Program No. 2015JM5158) and the Shaanxi Province Postdoctoral Scientific Research Project for partial financial support.

## References

- [1] J.W. Yan, X.F. Zhu, B. Yang, G.P. Zhang, Phys. Rev. Lett. **110**, 155502 (2013)
- [2] J.Y. Zhang, X. Zhang, R.H. Wang, S.Y. Lei, P. Zhang, J.J. Niu, G. Liu, G.J. Zhang, J. Sun, Acta Mater. **59**, 7368 (2011)
- [3] J.J. Niu, J.Y. Zhang, G. Liu, P. Zhang, S.Y. Lei, G.J. Zhang, J. Sun, Acta Mater. **60**, 3677 (2012)
- [4] Y.Y. Lu, R. Kotoka, J.P. Ligda, B.B. Cao, S.N. Yarmolenko, B.E. Schuster, Q. Wei, Acta Mater. **63**, 216 (2014)
- [5] R. Raghavan, T.P. Harzer, V. Chawla, S. Djaziri, B. Phillipi, J. Wehrs, J.M. Wheeler, J. Michler, G. Dehm, Acta Mater. **93**, 175 (2015)
- [6] Y.P. Li, G.P. Zhang, Acta Mater. **58**, 3877 (2010)
- [7] N. Jia, M.W. Zhu, Y.R. Zheng, T. He, X. Zhao, Acta Metall. Sin. (Engl. Lett.) **28**, 600 (2015)
- [8] S.L. Lehoczy, Phys. Rev. Lett. **41**, 1814 (1978)
- [9] J.Y. Zhang, S. Lei, J. Niu, Y. Liu, G. Liu, X. Zhang, J. Sun, Acta Mater. **60**, 4054 (2012)
- [10] Y.X. Zhao, W.S. Lai, Acta Metall. Sin. (Engl. Lett.) **25**, 141 (2012)
- [11] A. Misra, J.P. Hirth, R.G. Hoagland, Acta Mater. **53**, 4817 (2005)
- [12] J.Y. Zhang, X. Zhang, G. Liu, G.J. Zhang, J. Sun, Scr. Mater. **63**, 101 (2010)
- [13] Y.Q. Wang, J.Y. Zhang, X.Q. Liang, K. Wu, G. Liu, J. Sun, Acta Mater. **95**, 132 (2015)
- [14] P. Zhang, J.Y. Zhang, J. Li, G. Liu, K. Wu, Y.Q. Wang, J. Sun, J. Mater. Sci. **50**, 1901 (2014)
- [15] P. Zhang, J.Y. Zhang, J. Li, G. Liu, K. Wu, Y.Q. Wang, J. Sun, Acta Mater. **76**, 221 (2014)
- [16] R. Saha, W.D. Nix, Acta Mater. **50**, 23 (2002)
- [17] D. Pan, A. Inoue, T. Sakurai, M.W. Chen, Proc. Natl. Acad. Sci. **105**, 14769 (2008)
- [18] J.Y. Zhang, Y. Liu, J. Chen, Y. Chen, G. Liu, X. Zhang, J. Sun, Mater. Sci. Eng. A **552**, 392 (2012)
- [19] Y. Liu, D. Bufford, H. Wang, C. Sun, X. Zhang, Acta Mater. **59**, 1924 (2011)
- [20] Y. Chen, Y. Liu, C. Sun, K.Y. Yu, M. Song, H. Wang, X. Zhang, Acta Mater. **60**, 6312 (2012)
- [21] P.A. Gruber, J. Böhm, F. Onuseit, A. Wanner, R. Spolenak, E. Arzt, Acta Mater. **56**, 2318 (2008)
- [22] M. Chen, E. Ma, K.J. Hemker, H. Sheng, Y. Wang, X. Cheng, Science **300**, 1275 (2003)
- [23] J.Y. Zhang, G. Liu, R.H. Wang, J. Li, J. Sun, E. Ma, Phys. Rev. B **81**, 172104 (2010)
- [24] M. Wang, D. Wang, T. Kups, P. Schaaf, Mater. Sci. Eng. A **644**, 275 (2015)
- [25] H.J. Choi, S.W. Lee, J.S. Park, D.H. Bae, Scr. Mater. **59**, 1123 (2008)
- [26] H. Miyamoto, K. Ota, T. Mimaki, Scr. Mater. **54**, 1721 (2006)
- [27] A.J. Kalkman, A.H. Verbruggen, S. Radelaar, J. Appl. Phys. **92**, 6612 (2002)
- [28] R.W. Hayes, D. Witkin, F. Zhou, E.J. Lavernia, Acta Mater. **52**, 4259 (2004)
- [29] J.Y. Zhang, Y.Q. Wang, K. Wu, P. Zhang, G. Liu, G.J. Zhang, J. Sun, Mater. Sci. Eng. A **612**, 28 (2014)
- [30] P. Gu, M. Dao, R.J. Asaro, S. Suresh, Acta Mater. **59**, 6861 (2011)
- [31] Q. Wei, S. Cheng, K.T. Ramesh, E. Ma, Mater. Sci. Eng. A **381**, 71 (2004)
- [32] R.J. Asaro, S. Suresh, Acta Mater. **53**, 3369 (2005)